GPS Solutions (2023) 27:117
https://doi.org/10.1007/s10291-023-01432-6

ORIGINAL ARTICLE

Detection of GNSS antenna oscillatory motion and multipath conditions via exploitation of multipath-induced SNR variations

I. Peppa[1] · **P. A. Psimoulis**[1]

Received: 14 January 2020 / Accepted: 28 February 2023

Abstract
The multipath effect is well known as one of the dominant error sources in most high-precision GNSS applications, as its site-dependent and fast-changing nature render it challenging to model and mitigate using differencing techniques. However, in this study, we present a novel approach of using the multipath effect of GNSS signal in the case of oscillatory motion of a GNSS antenna to determine the characteristics of the oscillatory motion by utilizing the signal-to-noise (SNR) ratio measurements of the GNSS signals and without applying the positioning solution or the use of other sensors. The proposed method is based on the hypothesis that for a short time period, while the multipath conditions remain constant and the satellites are approximately at the same position, an oscillation-type motion of the antenna should generate changes in multipath, expressed as oscillatory pattern variations in the SNR measurements of the satellites. This approach can be used to identify the multipath parameters and extract characteristics of the oscillatory motion of the GNSS antenna. The SNR-based modeling of cm-level antenna oscillations was demonstrated in simulated and field experiments. The benefits of this method include immunity to poor satellite constellation geometry, adaptability to changing multipath geometry and fast processing time. This approach could potentially, under conditions, contribute to GNSS reflectometry (GNSS-R) applications, where the oscillatory motion of the GNSS antenna generates the same effect as the satellite motion-induced multipath, limiting simultaneously the observation periods and the amount of data to be processed.

Keywords Multipath · SNR · Simulator · Antenna oscillatory motion · Remote sensing

Introduction

Multipath is one of the major error sources in GNSS positioning, significantly affecting GNSS navigation (Hsu et al. 2015) and deformation monitoring applications (Stiros et al. 2019). Especially, in monitoring of major civil engineering structures response, such as long-span bridges, where GNSS measurements play a significant role in the estimation of the characteristics of structure response (amplitude and frequency; Msaewe et al. 2021), under conditions of extreme loading (Meng et al. 2019).

One of the main parameters to monitor the potential multipath effect for each GNSS satellite is the signal-to-noise ratio (SNR), which primarily indicates the signal strength and the noise density of the received satellite signal (Strode and Groves 2016). The SNR data derive from the composite signal (i.e., direct and reflected satellite signals) and reflect any distortion of the correlation function due to constructive or destructive multipath interference (Hsu et al. 2015). Common multipath mitigation techniques involve the integration of GNSS with other sensors (Moschas et al. 2013) and filtering the frequencies, which include the multipath frequency band (Psimoulis and Stiros 2012). The latter is a common technique in structural health monitoring, which, however, may remove the information on the structure response corresponding to low frequencies (Peppa et al. 2018). SNR-based phase multipath estimation and mitigation techniques (Betaille et al. 2006; Lau and Cross 2007; Strode and Groves 2016) use the multipath effect on SNR to estimate the multipath characteristics and mitigate the code and carrier phase errors.

In recent studies, the multipath effect on GNSS satellite signals has become a tool as it is employed in mapping the multipath environment (Bilich and Larson 2007) and GNSS remote sensing applications (Roussel et al. 2016;

✉ P. A. Psimoulis
panagiotis.psimoulis@nottingham.ac.uk

[1] Nottingham Geospatial Institute, The University of Nottingham, Nottingham, UK

Published online: 26 April 2023

Wei et al. 2019; Steiner et al. 2019), where the SNR is analyzed to identify variations of (1) moisture and soil parameters (Chew et al. 2014; Wu et al. 2018), (2) the tides and the mean sea level (Lofgren et al. 2014; Jin et al. 2017) and (3) the snow height (Larson and Nievinski 2013). The principle of those studies is that the GNSS antenna remains stable for the recording period and the SNR variations are the result of the satellite orbit and the reflection point as it moves across the reflecting surface, while day-to-day variability is the result from changes of the multipath environment.

For the hypothesis of this study, we reverse the above principle and assume that for a very short period (i.e., about 1 min), the GNSS satellite is considered still at its trajectory and the multipath conditions do not change. Hence, the potential oscillation-type motion of the GNSS antenna for a short period is the main driver for temporary changes in the multipath conditions, expressing the variation of the antenna–reflector distance, and which should be reflected in the SNR of the GNSS satellites signal. By analyzing the SNR satellite time series, the characteristics of the GNSS antenna oscillation-type motion could be estimated. This hypothesis has been described by Braasch (2017), without, however, following by further investigation, theoretical, analytical or experimental applied to GNSS measurements. The first evidence of this hypothesis was presented by Peppa et al. (2018), who estimated (1) the frequency of an oscillated GNSS antenna in controlled experiments and (2) the main modal frequency of the Wilford Suspension Bridge in Nottingham, UK, by analyzing the SNR of GPS satellites signal. In both cases, the oscillation-type waveform of the SNR satellites signal for the short period of the imposed excitation was evident (i.e., 1 min).

In this study, an attempt has been made to model the multipath effect in the SNR for a short term vertical oscillatory motion of GNSS antenna and estimate the antenna oscillation characteristics and the multipath conditions. Firstly, an analytical model is developed to describe the SNR variations, which are induced through multipath and generated by GNSS antenna oscillatory motion, and evaluate the impact of the multipath parameters. Then, the analytical model is validated and evaluated based on simulated and experimental GNSS data, for vertical GNSS antenna oscillatory motion. This study leads to a novel approach, which can potentially broaden the applications in deformation monitoring and GNSS reflectometry (GNSS-R), and enhance the GNSS positioning for complex multipath environments. Since the scope of this study was to prove the main hypothesis and develop a model relating SNR with the GNSS antenna oscillation-type motion, we focused only on GPS satellites and the impact on their SNR time series.

Modeling SNR and carrier phase multipath for short-term antenna oscillation

The multipath effect occurs when the direct signals from the satellites interfere with those reflected from objects in the vicinity of the antenna. Objects with large, smooth surfaces (e.g., ground, wall, water/metal surface) produce specular reflections which have a significant impact on the positioning solution. The reflected signal that produces interference is characterized by; (1) the path delay, δ (in meters), (2) reflected signal amplitude, A_m (in volts), (3) the relative multipath phase with respect the direct signal, ψ (in radians), (4) the relative phase rate and (5) the polarization with respect the direct signal. Following Snell's law, the angle of incidence of the reflected signal equals to the angle of reflection. Thus, for horizontal reflections, the path delay, δ, of the reflected signal is related to the height of the antenna, H (in meters), and the satellite elevation angle, θ (in degrees), expressed through the following relationship (Fig. 1):

$$\delta = 2H \sin(\theta) \tag{1}$$

or

$$\delta = 2H \sin(\theta - \gamma) \tag{2}$$

for the general case, where γ is the inclination angle of the reflector (in degrees).

The interference of the reflected signal(s) with the direct signal results to the composite signal. The SNR, which is affected by many errors (i.e., atmospheric errors, receiver noise, etc.), among them the multipath, is a function of the composite signal amplitude, A_c. By applying the geometric

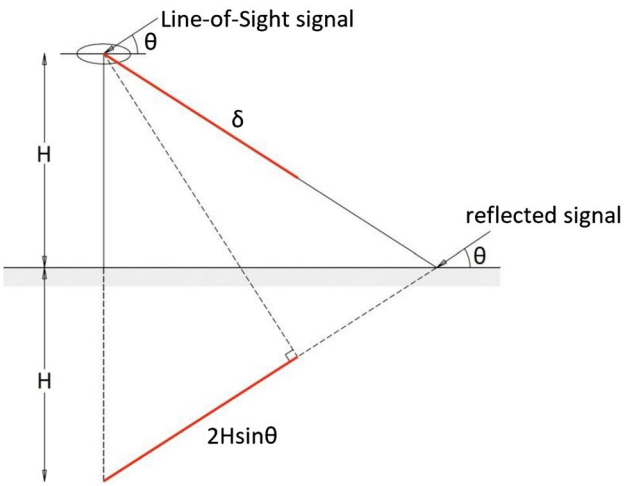

Fig. 1 Multipath geometry of a GNSS antenna with a planar and horizontal ground reflection ($\gamma = 0$), with antenna–reflector distance H, and satellite elevation angle θ

relations of the phasor diagram that express the direct (A_d), reflected (A_m) and composite signal (A_c), we can express SNR as (Bilich et al. 2008):

$$\mathrm{SNR}^2 \equiv A_c^2 = A_d^2 + A_m^2 + 2A_dA_m \cos\psi \tag{3}$$

where the amplitude of all signals is in volts. Furthermore, the relative multipath phase, ψ, is the angular equivalent to the additional path length, δ, and it can be expressed as follows (Bilich et al. 2008; Braasch 2017):

$$\psi = \frac{2\pi}{\lambda}\delta = \frac{2\pi}{\lambda}2H\sin(\theta - \gamma) \tag{4}$$

For the case of one dominant reflector and SNR time series of short time interval (~ 1 min), Eq. (3) can be simplified to (Bilich et al. 2008):

$$\mathrm{SNR} = A_d + A_m\cos\psi + \varepsilon \tag{5}$$

where SNR is the result of (1) the direct signal of amplitude A_d, (2) the reflected signal, expressed as a periodic function of the multipath relative phase ψ and multipath amplitude A_m and (3) the noise ε of the SNR observables. Two points that need to be clarified are that (1) the amplitude of the direct signal is significantly larger than that of the multipath amplitude ($A_d >> A_m$) and (2) for a long time interval of SNR time series, the direct signal component has a long-period effect which is usually detrended by using a polynomial fit, and the remaining offset due to the imperfect nature of the polynomial fit is expressed by the term A_d (A_o in Bilich et al. 2008). However, for a short time interval of SNR time series (e.g., 1 min), such as those examined in this study, the long-period effect of the direct signal is limited and the impact of the direct signal, A_d, can be assumed as constant or slowly varying linearly with time, whereas the second term expresses the variations of the SNR time series, as it is governed by the change rate of multipath relative phase ψ which is driven by the oscillatory motion.

The motion of the satellites along their orbits produces the sinusoidal pattern of the SNR time series, where the frequency depends on the antenna–reflector distance (Strode and Groves 2016). However, for the case of the oscillatory motion of a GNSS antenna for a very short period (e.g., 1 min), where the satellite motion along its orbit is null, and the parameters θ and γ can be assumed constant with respect the antenna motion, the reflection point oscillates across the reflector, following the motion of the antenna (Fig. 2). For the vertical oscillatory motion of the GNSS antenna, the equation of the antenna–reflector perpendicular distance, H, is:

$$H(t) = H_o + \left(A_{\mathrm{mot}}\cos\gamma\right)\cdot\sin 2\pi ft \tag{6}$$

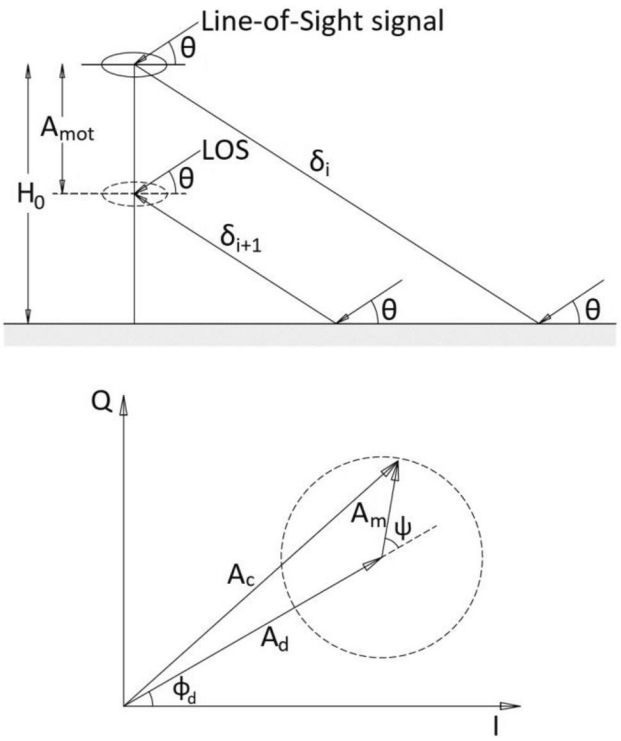

Fig. 2 (top) Geometry of planar and horizontal ground reflections ($\gamma = 0$) for a GNSS antenna which executes a vertical oscillatory motion. For a short time interval, the path delay variations are mainly driven by the antenna height variations. (bottom) Phasor diagram representing the carrier tracking loop operation and the relationship between the in-phase (I) and quadrature-phase (Q), with the vectors of the direct (A_d), multipath (A_m) and combined (A_c) signals and the relative multipath phase, ψ. The two peripheral arrows indicate the oscillation of the multipath phasor due to the antenna oscillation (modified after Bilich and Larson 2007)

where H_o is the antenna–reflector distance for the equilibrium position (in meters), A_{mot} is the amplitude of the oscillation (in meters) and f is the oscillation frequency (in Hz). The antenna motion introduces variations in ψ and SNR, forming the following equations:

$$\psi = \frac{4\pi}{\lambda}\left(H_o + \left(A_{\mathrm{mot}}\cos\gamma\right)\cdot\sin 2\pi ft\right)\cdot\sin(\theta - \gamma) \tag{7}$$

$$\mathrm{SNR}(t) = A_d + A_m\cos\left[\frac{4\pi}{\lambda}\left(H_o + \left(A_{\mathrm{mot}}\cos\gamma\right)\cdot\sin 2\pi ft\right)\cdot\sin(\theta - \gamma)\right] + \varepsilon \tag{8}$$

where the relative multipath phase and the SNR time series are expressed as a function of the antenna oscillatory motion.

Based on (8) and for a short period (i.e., 1 min), it can be assumed that (1) the satellite elevation angle θ and the multipath conditions (A_m, γ and H_o) remain constant, and (2) the direct signal amplitude A_d can be modeled by applying a linear function (as explained above a polynomial fit is

used for the long-period effect of direct signal in SNR; see Bilich et al. 2008). Therefore, the impact of the oscillation motion (A_{mot},f) of the GNSS antenna should be reflected on the SNR time series. In the current study, the raw data of SNR were converted from dB-Hz to the linear unit volts, V, to measure the SNR composite signal and apply (7) and (8).

Analysis of the SNR dependency on the multipath geometry and antenna motion characteristics

Based on the model of (8), we examined the effect of the multipath conditions and the antenna motion characteristics on the SNR time series. More specifically, we analyzed the impact of (1) the antenna–reflector distance H_o, (2) the satellite elevation angle θ and (3) the antenna oscillation amplitude A_{mot}, on the SNR time series for the case of the vertical oscillatory motion of the GNSS antenna, and a planar, horizontal reflector (i.e., $\gamma = 0$) to simplify the geometry between satellite-receiver-reflector. We also examined the impact of the reflection angle (i.e., $\theta - \gamma$) on the SNR variations phase difference with respect to the antenna oscillation motion. For this analysis, we did not consider the antenna gain pattern effect on the SNR time series, as it is antenna-specific, and the aim is to investigate the impact of the antenna motion on the SNR time series regardless the type of the antenna (i.e., antenna gain pattern).

Apart from the sinusoidal pattern on the SNR time series due to the satellite motion (Bilich et al. 2008), the antenna oscillation creates a superimposed effect on the SNR time series, which has a sinusoidal pattern defined by the frequency of the antenna motion. This can also be represented by the phasor diagram in Fig. 2, where the satellite motion along its orbit results in the multipath phasor A_m to spin slowly, while the oscillatory antenna motion causes the multipath phasor A_m to oscillate around its equilibrium position (indicated by the peripheral arrows in Fig. 2), with the same frequency as the antenna oscillation, concurrently to this slow spin. Figure 3 presents the analytical residual SNR time series, i.e., after removing the direct signal contribution, for various antenna–reflector distances, where the amplitude and frequency of the antenna oscillation are 1 cm and 0.5 Hz, respectively, and the satellite elevation angle ranges between 28° and 31°. Apart from the dominant effect of the satellite motion in the frequency of the SNR time series (i.e., the slow spin of the multipath phasor), there are also observed variations of smaller amplitude and higher frequency corresponding to the antenna oscillation (i.e., oscillation of multipath phasor). The frequency of the SNR oscillation due to the satellite motion effect increases significantly for large antenna–reflector distance, approaching the one of the antenna motion effect,

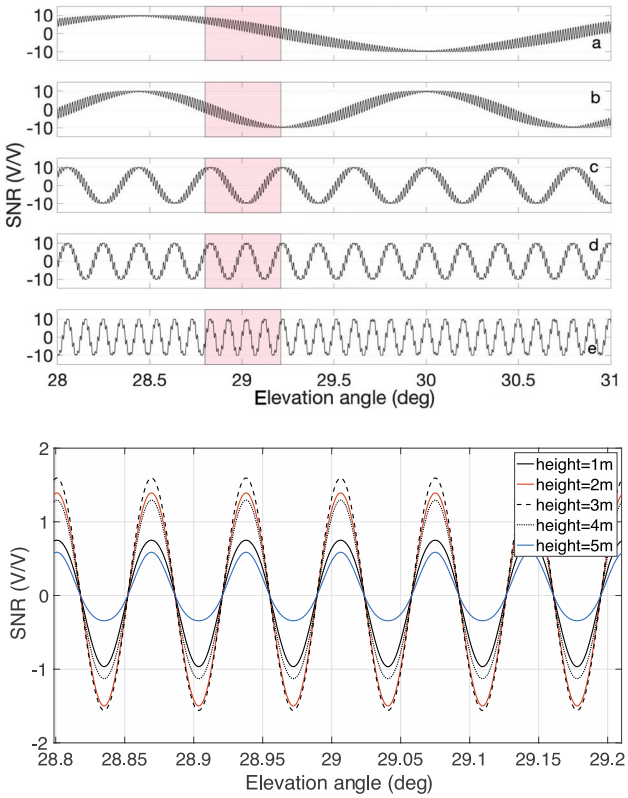

Fig. 3 (top) Residual SNR time series for antenna–reflector vertical distance of **a** 2 m, **b** 4 m, **c** 16 m, **d** 32 m and **e** 64 m, and antenna oscillation of 1 cm and 0.5 Hz. The 1-min interval is highlighted. (bottom) Residual SNR time series, of the 1-min interval, extracted after removing the initial trend due to the satellite motion and corresponding to satellite elevation angle from 28.8° to 29.2°

making the separation of the two superimposed patterns challenging. For relatively short antenna–reflector vertical distance (e.g., 2–4 m), the trend due to the satellite motion effect can be removed without distorting the SNR pattern due to the antenna oscillation. The 1-min period of the antenna oscillation-generated SNR pattern was extracted from the initial SNR time series (Fig. 3-bottom), corresponding to antenna–reflector distance between 1 and 5 m and the satellite elevation angle in a range of 0.4° was assumed constant. The residual SNR amplitude varies between 0.5 and 1.5 V with the antenna–reflector distance, driven by the $\cos\psi$.

By applying a similar approach, we examined the amplitude variance of the SNR residual time series caused by the antenna oscillation as a function of the satellite elevation angle. As seen in Fig. 3 (top), the amplitude of the antenna oscillation—induced SNR variations is not fixed; it minimizes at intervals coinciding with the crests and troughs of the dominant SNR variation due to the satellite motion and maximizes in-between.

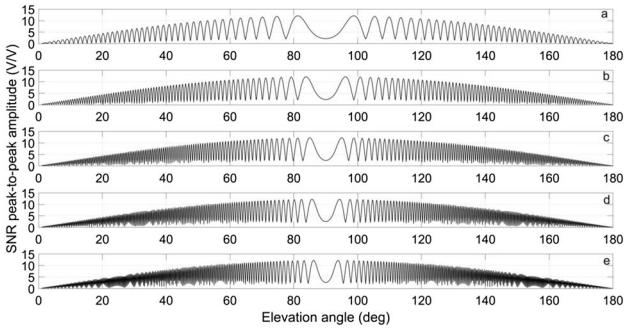

Fig. 4 Residual SNR peak-to-peak amplitude against the elevation angle of the satellite with a horizontal reflector and perpendicular distances between antenna and reflector of **a** 2 m, **b** 4 m, **c** 6 m, **d** 8 m and **e** 10 m. The antenna motion amplitude and antenna motion frequency are 1 cm and 0.1 Hz, respectively. For this example, $A_d = 100$ V and $A_m = 10$ V

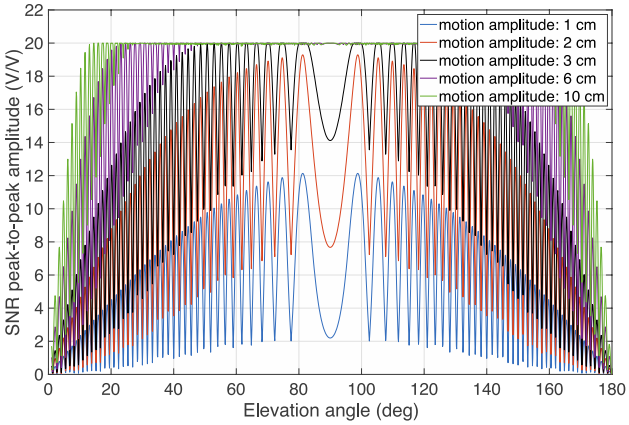

Fig. 5 Residual SNR peak-to-peak amplitude against the elevation angle of the satellite for oscillation amplitude between 1 and 10 cm

Figure 4 shows the variation of the SNR peak-to-peak amplitude with the elevation angle for various antenna–reflector distances. The derivation of the SNR peak-to-peak amplitude is explained explicitly in Electronic Supplement and Figures S1–S4. The SNR peak-to-peak amplitude variations are of higher frequency for low-elevation angles in the same way that a low-elevation satellite will produce a higher frequency SNR multipath pattern in a stable antenna (Bilich and Larson 2007). In a superimposed effect of concurrent satellite and antenna motion, the rate of change of the elevation angle does not affect the frequency of the SNR time series, as is the case for a stable antenna, since the frequency of the SNR time series is driven by the frequency of the antenna motion. Instead, it affects the rate of change of the amplitude of the SNR oscillations. Likewise, the SNR amplitude variations are more frequent for large antenna–reflector distances in the same way large antenna–reflector distances produce higher frequency SNR multipath oscillations in a stable antenna (Bilich and Larson 2007). The general trend also shows that the maximum SNR peak-to-peak amplitude increases with the satellite elevation angle, as it is driven by the $\sin(\theta)$ in the relative multipath phase (5), as the reflector was considered planar and horizontal ($\gamma = 0$). Since this analysis is free of antenna gain pattern effects, the above observations are only due to the satellite–antenna–reflector geometry; by adding the antenna gain pattern effect, would limit the maximum SNR peak-to-peak amplitude for high satellite elevation angles, depending on the antenna-specific gain pattern.

On the other hand, examining the SNR peak-to-peak amplitude for various antenna oscillation amplitudes A_{mot} (1–10 cm) shows that the SNR amplitude fluctuations show the same pattern. The maximum value increases with the antenna oscillation amplitude A_{mot} (Fig. 5). For instance, for an oscillation amplitude of 1 cm and 10 cm, the maximum SNR amplitude is 12.3 and 20 V, respectively. Also, the larger the oscillation amplitude, the smaller is the elevation angle for which the maximum SNR amplitude will be reached; for instance, for 3 and 10 cm oscillation amplitude, the maximum SNR amplitude is achieved for elevation angles of 44° and 16°, respectively. The maximum threshold, 20 V, is determined by the multipath intensity; in real application, it will depend on the reflection coefficient of the reflector and the antenna gain pattern attenuation. Besides, the antenna oscillation amplitude also affects the waveform of the SNR multipath time series, as the SNR time series has a more complex waveform for large antenna oscillation amplitude (i.e., > 10 cm), for the given antenna–reflector distance (Fig. S5).

Regarding the phase difference between the SNR multipath oscillation pattern and the antenna oscillation, it was observed by Peppa et al. (2018) that the phase between the two time series differs either by zero or π (see Fig. 9, 11 in Peppa et al. (2018)). The phase difference depends on the reflection angle, which is formed by (1) the geometry between the satellite elevation angle (θ) and the reflector inclination angle (γ), (2) the reflector–antenna distance (H_o) and (3) the oscillation amplitude (A_{mot}). Focusing on the reflection angle, as it continuously changes due to the satellite trajectory, four different back-scatter and forward-scatter multipath cases are generated based on the relationship between θ and γ (Fig. S6; Peppa, 2020). By correlating the SNR multipath time series with the antenna oscillation time series, it is proved that the phase shift depends on the reflection angle (Fig. 6). There are frequent alternations of the phase shift between zero and π for small reflection angles, which are reduced with the reflection angle, finally leading to a zero phase shift between 78° and 90°. The latter practically means that if a satellite with high elevation

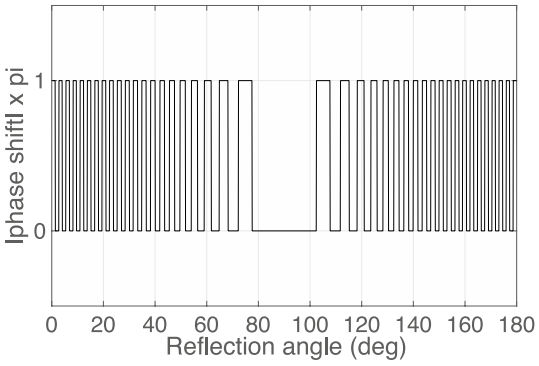

Fig. 6 Phase shift between residual SNR and antenna oscillation time series, alternating between 0 and π with the reflection angle

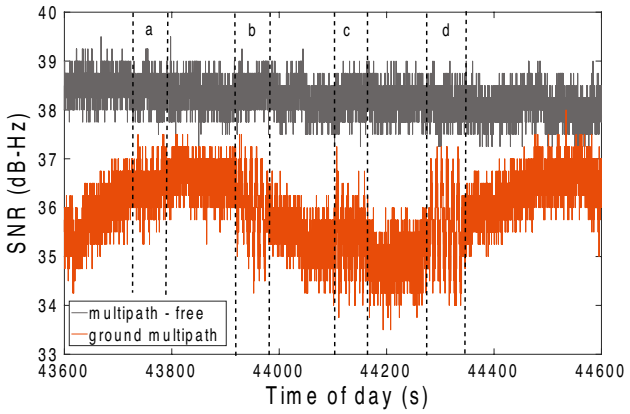

Fig. 7 SNR time series for PRN11 in a multipath-free (top-gray) and ground multipath (bottom-red) simulated environment. The antenna motion corresponds to vertical oscillations of 0.1 Hz with amplitudes of **a** 1 cm, **b** 2 cm, **c** 3 cm and **d** 4 cm. The multipath-free SNR time series have been offset for clarity

angle has variations in its SNR in-phase with the antenna motion, then the reflector is probably horizontal underneath the antenna (e.g., ground). In Electronic Supplement can be found more details about the phase difference between SNR and oscillation amplitude and the impact of antenna–reflector distance (Fig. S7).

Analysis of simulated SNR time series for antenna vertical oscillations

The simulations aim to validate the accuracy and robustness of the analytical model between the SNR time series and the GNSS antenna oscillation by introducing hardware noise derived from the GNSS receiver. Further, the effect of the oscillation characteristics, the multipath intensity and the antenna gain pattern on the effectiveness of the SNR model was examined.

The GNSS simulations were conducted by using the GSS8000 GNSS hardware simulator, the signal of GPS satellites and the ground as the only source of the simulated multipath. The ground is simulated as a horizontal homogeneous surface underneath the antenna. Simulations with activated ionospheric and tropospheric effects did not show any influence, thus were not further used in the simulations. A Triumph-1 Javad receiver recording at 10 Hz was used for the GPS data simulations, and the location of the antenna was simulated as being at the Nottingham Geospatial Institute (NGI), 1.6 m above the ground.

Figure 7 presents the simulated SNR time series with and without activating ground motion for various cases of antenna oscillation. For the multipath-free environment, the SNR time series is characterized by a constant average, with the variations reflecting only the noise of the simulator and the GNSS receiver. The multipath-contaminated SNR time series consist of two superimposed patterns; (1) the slowly varying sinusoidal pattern due to the satellite elevation angle changes and (2) the oscillation pattern occurring during the intervals of antenna oscillation. Hence, the oscillation-pattern component of the SNR is due to the oscillation-induced multipath since no oscillation-pattern signal occurred in SNR for a multipath-free environment.

Several simulations were designed to investigate the fit of the model for antenna oscillations of different characteristics (amplitude and frequency), different satellite signal attenuation and the impact of the satellite elevation angle and antenna radiation pattern. For the validation of the analytical model, the following methodology was followed:

Step 1: The relative multipath phase for each oscillation is constructed using (7) and the pre-defined parameters of the multipath conditions: (1) elevation angle θ, (2) the GPS $L1$ signal wavelength, (3) the reflector inclination angle γ, (4) the antenna–reflector distance H_o and (5) the antenna oscillation characteristics (amplitude, frequency).

Step 2: For the given multipath relative phase, the model of (5) is applied on the simulated SNR time series to estimate the reflected and the direct signal amplitude, A_{m} and A_{d}, respectively, by using the nonlinear least-squares method.

Step 3: The effect of the oscillation characteristics and the multipath intensity is evaluated based on the goodness of the model fit, and the estimation of the multipath signal amplitude A_{m}. The goodness of the SNR model fit expresses the effect of the hardware noise on the motion-generated SNR pattern.

It should be noted that the values of the antenna–reflector distance and the antenna oscillation characteristics in Step 1 were considered as known to construct the relative multipath phase when examining the effect of the antenna oscillation characteristics and the multipath intensity, as the aim was to evaluate the robustness of the SNR modeling for

different types of antenna motion and multipath intensity in the presence of hardware receiver noise. The effectiveness of the SNR model in real conditions was examined in the experiments of vertical oscillation-type movement of the GPS antenna.

Effect of antenna oscillation characteristics

In Fig. 8 are presented the SNR time series corresponding to oscillations of amplitude between 10 and 40 mm and frequency between 0.1 and 2 Hz. Generally, the fit of the model is improved when the oscillation amplitude and the oscillation frequency increase and decrease, respectively. For small oscillation amplitudes, the SNR variations are minor and mainly masked from the SNR time series noise, whereas for relatively high-frequency oscillations (1–2 Hz) with large oscillation amplitude, the relatively poor SNR resolution (i.e., 0.1 dB) cannot reflect precisely the oscillation pattern in the SNR time series. The latter is also revealed from the spectral analysis of the SNR time series (Fig. 9). The fit of the model, expressed through the correlation coefficient (R^2), to the simulated data is improved as the oscillation frequency decreases and especially for oscillation amplitude of 30–40 mm; for 0.1 Hz and 0.5 Hz the correlation coefficient is $R^2 > 0.9$ and $R^2 > 0.7$, respectively, while for oscillation frequency of 2 Hz, the correlation coefficient is very low (i.e., $R^2 < 0.5$; Fig. S8).

Effect of multipath intensity on SNR time series

Another series of simulated oscillations was conducted for three cases of reflected signal attenuation, 10 dB, 20 dB and 30 dB, with oscillation amplitude ranging from 5 to 40 mm and an oscillation frequency of 0.1 Hz. The simulations were made for the same satellites and intervals of their orbits. Based on the SNR model, the SNR amplitude is proportional to the multipath intensity, represented by the reflected signal amplitude A_m. Thus, the SNR amplitude

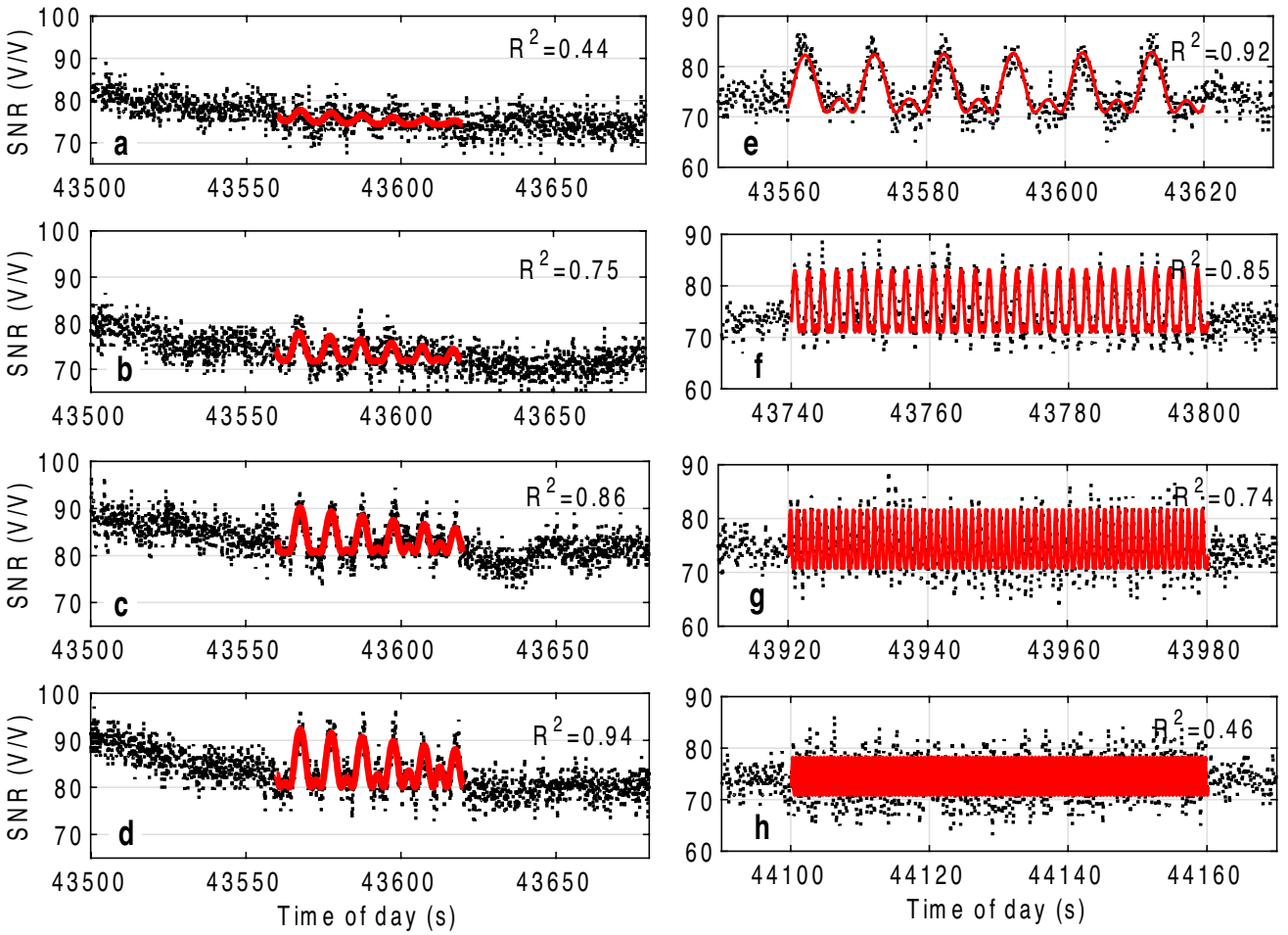

Fig. 8 SNR time series and the fit of the model, for simulated vertical antenna oscillation of (left) amplitude **a** 1 cm, **b** 2 cm, **c** 3 cm and **d** 4 cm and frequency 0.1 Hz and (right) amplitude 20 mm and frequency **e** 0.1 Hz, **f** 0.5 Hz, **g** 1 Hz and **h** 2 Hz

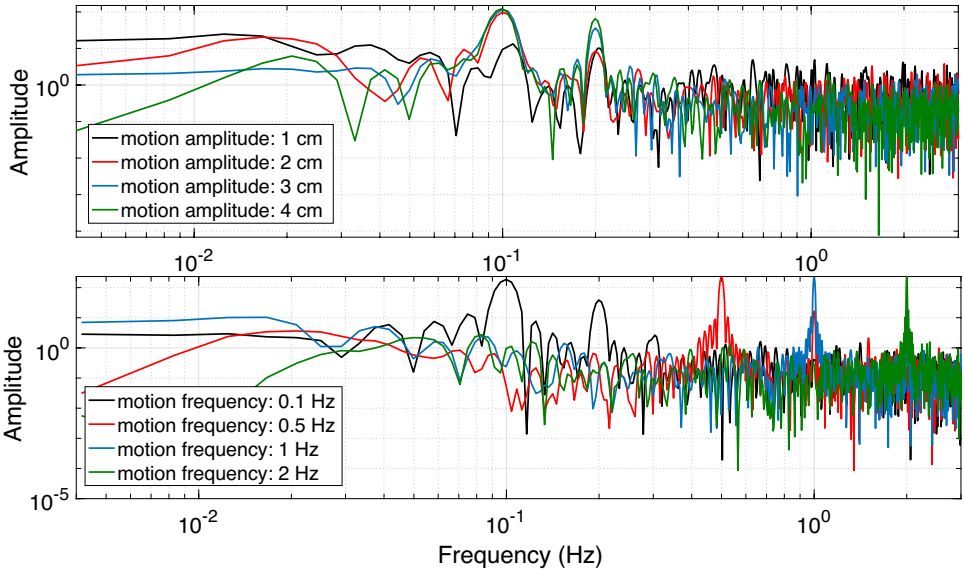

Fig. 9 Spectral analysis of the SNR time series with (top) oscillation frequency of 0.1 Hz and amplitude ranging between 1 and 4 cm and (bottom) oscillation amplitude of 20 mm and frequency ranging between 0.1 and 2 Hz

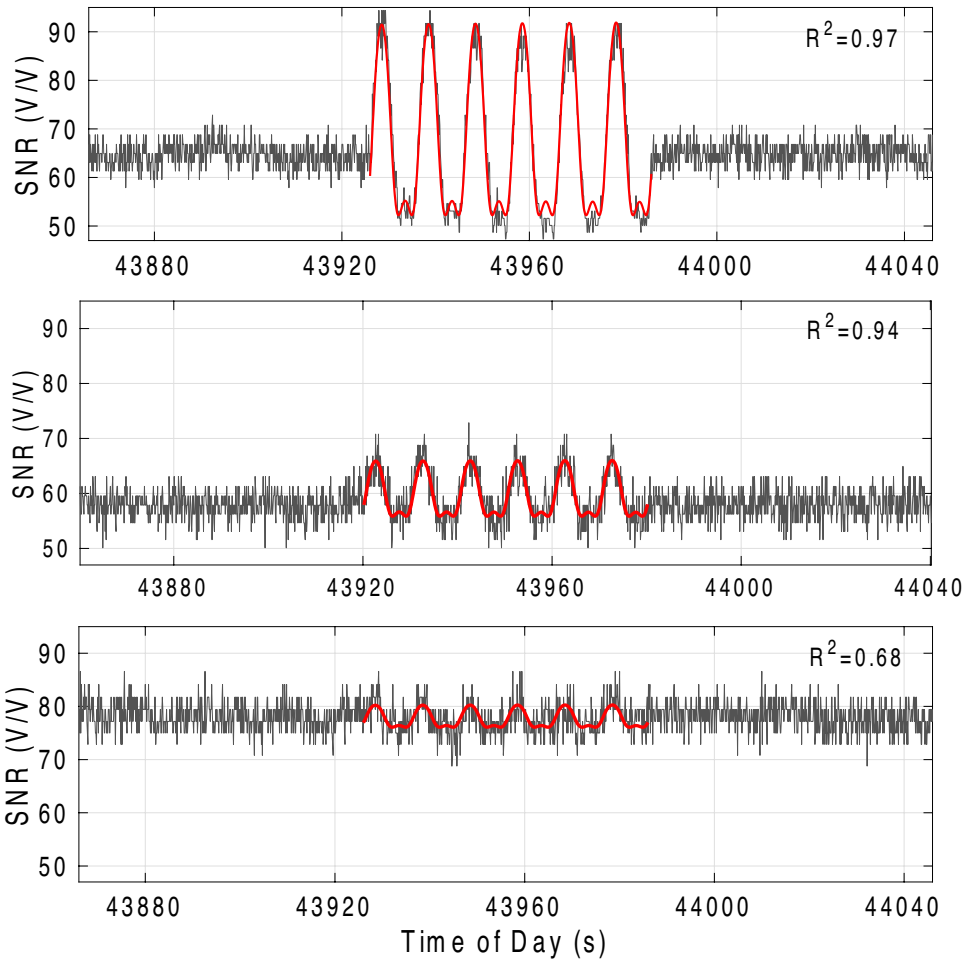

Fig. 10 SNR time series and the fit of the model for antenna oscillation of amplitude 20 mm, frequency 0.1 Hz and reflection attenuation (top) 10 dB, (middle) 20 dB and (bottom) 30 dB

should be reduced for reflection of strong attenuation, considering all other parameters unchanged. Figure 10 presents the SNR time series for an antenna oscillation simulation (20 mm amplitude, 0.1 Hz frequency) corresponding to the three examined signal attenuations. The fit of the model is improved as the signal attenuation decreases; for 10 dB,

20 dB and 30 dB, the correlation coefficient is 0.97, 0.94 and 0.68, respectively. Furthermore, the correlation coefficient seems to have more spread for the 20 and 30 dB reflection attenuation, as in these cases, the fit of the model depends on the oscillation characteristics (amplitude, frequency, etc.), while for the 10 dB attenuation, the fit of the model is excellent ($R^2 > 0.9$), regardless the oscillation amplitude, as the SNR pattern is amplified significantly by the multipath interference (Fig. S9).

Effect of antenna radiation pattern on SNR time series

To investigate the impact of the antenna radiation pattern on the antenna oscillation-generated SNR pattern, the SNR time series of a 4-h satellite orbit was analyzed, while antenna oscillations of specific characteristics were simulated. Vertical antenna oscillations (30 cm, 1 Hz) of 1-min time interval were simulated repeatedly during the 4-h SNR time series of the PRN 25 satellite, corresponding to elevation angle from 0° to 70°. The ground reflection was fixed to 20 dB, and the antenna radiation pattern resembles the Leica AS 10 GNSS antenna. Figure 11 presents the SNR time series with respect the satellite elevation angle, expressing the two multipath-induced effects: (1) the slow varying pattern produced by the satellite trajectory and (2) the fast, intermittent oscillatory pattern created by the antenna oscillations. Both effects are more dominant for low satellite elevation angles, getting more subtle and finally disappearing for high elevation angles due to the attenuation of the reflected signals from the antenna radiation pattern. Apart from the direct and the reflected-to-direct signal amplitude (attenuation factor α), the antenna–reflector vertical distance H_o and the oscillation amplitude A_{mot} were also treated as unknown parameters in the model and estimated (Step 2 of the methodology).

The direct (A_{d}) and the reflected (A_{m}) signal amplitude increases and decreases, respectively, with the satellite elevation due to the antenna radiation pattern effect (Fig. 12a, b). The derived attenuation factor α decreases with the elevation, following a parabolic trend, in agreement with previous studies (Bilich 2006). The oscillation amplitude (A_{mot}) is on average estimated with millimeter precision for the simulated oscillations corresponding to satellite elevation angle lower than 58°. For higher elevation angles, the antenna radiation pattern suppresses the reflected signal, leading to poorly reflected oscillations in the SNR time series. The antenna–reflector distance estimations vary intensely (Fig. 12d), since a good fit can be achieved for several values of antenna–reflector distance in the model. This fact is demonstrated by computing the maximum absolute SNR time series difference between a reference SNR model of 0.3 m motion amplitude and 1.6 m antenna–reflector distance and generated SNR models for motion amplitudes between 0.01 and 1 m (Fig. 12e) and antenna–reflector distance between 1.5 and 3 m (Fig. 12f), with a resolution of 1 cm in both cases. The difference for the oscillation amplitude minimizes only for the correct oscillation amplitude (i.e., 30 cm), while for the antenna–reflector distance, there are multiple minima, differing by approximately 0.5 m (Fig. 12e, f). Therefore, the multiple possible solutions for the antenna–reflector distance lead the SNR model to converge for each oscillation to a different value.

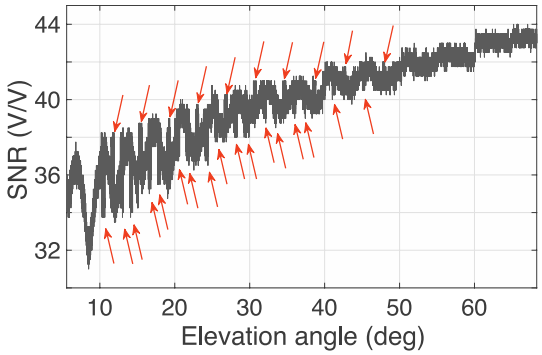

Fig. 11 SNR time series of the PRN 25 satellite for the 4-h period. The arrows indicate the visually identified periods which correspond to antenna oscillations

Experimental investigation of the SNR model for the oscillations of GNSS antenna

To assess the reliability of the SNR model, a series of experiments carried out on the roof of the NGI, where a geodetic antenna (Leica AS10), mounted on a heavy-duty tripod, could execute a vertical motion through a manually rotating handle. A full clockwise turn of the handle was measured to move the antenna vertically by 1.5 cm. The GNSS antenna was connected to a Leica GS10 receiver, recording at 10 Hz sampling rate. A GNSS base station consisted of the same type antenna and receiver, was recording also at 10 Hz. A Robotic Total station (RTS; Leica TS30) tracked a reflector connected to the GNSS antenna on the tripod and recorded its motion to confirm the exact amplitude and frequency of the oscillations, an approach applied successfully in previous experimental studies (Psimoulis and Stiros 2012). The tripod was set at $H_o = 1.6$ m vertical distance from the roof surface, and vertical oscillations were executed with amplitude and frequency ranging between 5–15 mm and 0.1–1 Hz, respectively. The duration of each oscillation was 1 min. For more details regarding the experimental layout of the GNSS antenna vertical oscillatory motion, the execution

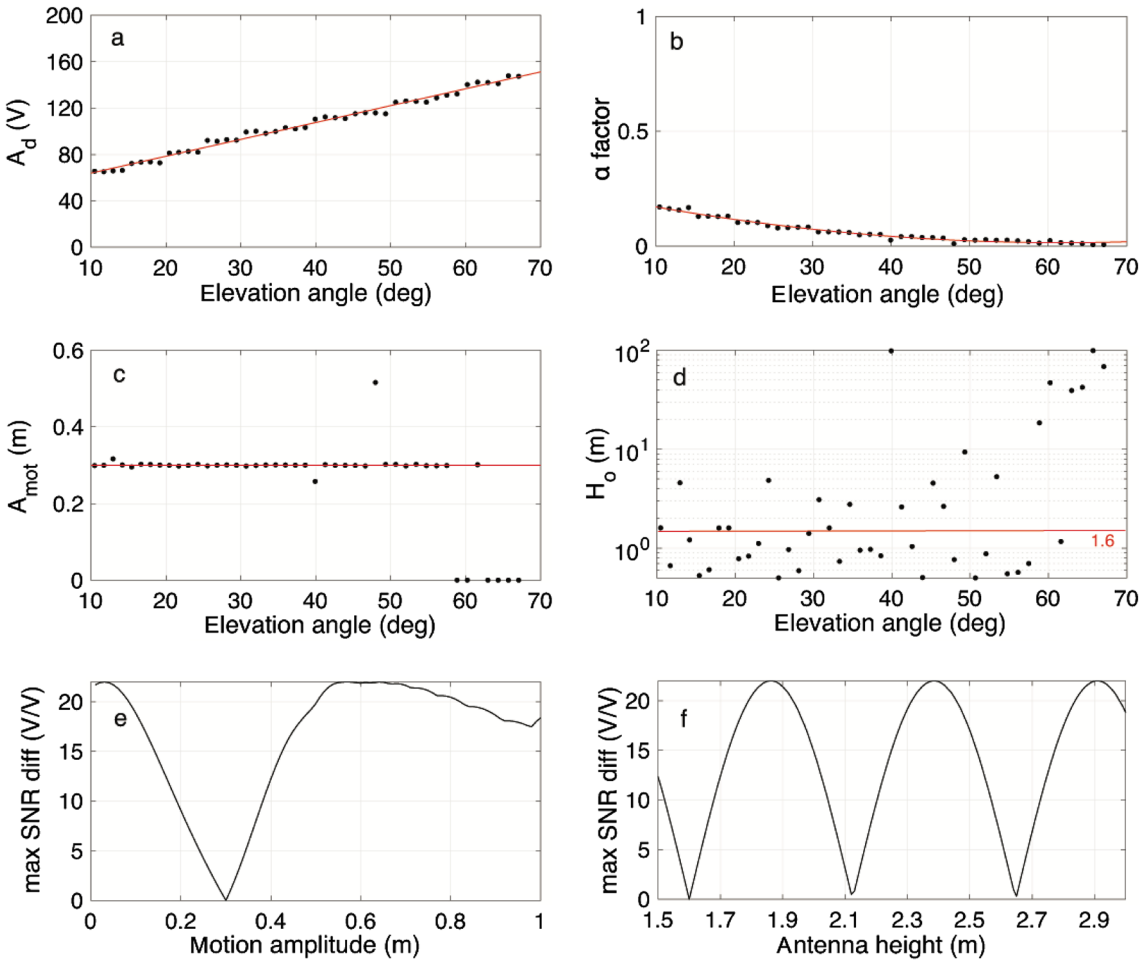

Fig. 12 Estimated values (black dots) of the **a** direct signal amplitude A_d, **b** attenuation factor α, **c** antenna oscillation amplitude A_{mot}, and **d** antenna–reflector vertical distance H_o, derived from the analysis of the simulated SNR time series corresponding to the 4-h satellite orbit, plotted against the satellite elevation angle. The red lines express the amplitude of the oscillations (i.e., $A_{mot}=0.3$ m) and the antenna–reflector distance ($H_o=1.6$ m). Also, the maximum absolute difference between the modeled and the reference SNR time series of oscillations with an amplitude 0.3 m and antenna–reflector distance 1.6 m is presented for solutions of different **e** motion amplitudes and **f** antenna heights

of the experiments and the assessment of GPS and RTS coordinate time series can be found in Peppa et al. (2018).

Two cases were examined for the antenna oscillation experiments, where the constraints and the unknown parameters were defined to represent the conditions of two potential GNSS applications: (case A) a GNSS reflectometry application and (case B) a structural health monitoring application. For case A, the antenna oscillatory motion was considered controlled (known oscillation amplitude and frequency), and the aim was to model the multipath conditions (A_d, α, H_o, γ). For case B, the multipath parameters were partly constrained based on the surrounding environment topography, and the oscillation-type motion of the GNSS antenna was considered unknown. The aim of case B was to model the multipath conditions (A_d, α, H_o, γ) and estimate the oscillation characteristics (A_{mot}, f). A similar methodology to that of simulations was followed, where different parameters were unknown per case. Only the 1 min of the SNR time series, where the antenna experienced vertical oscillations, was analyzed. The 1 min of the SNR time series, where the antenna experienced vertical oscillations, was analyzed using a spectral analysis technique to identify the antenna oscillation frequency.

Case A: modeling the multipath conditions

For the case of the known oscillation characteristics, the oscillation amplitude is derived from the RTS measurements, whereas the oscillation frequency is identified from the spectral analysis of the SNR, which proved successful (Peppa et al. 2018). However, the detection of the oscillation frequency becomes more challenging for small oscillation amplitudes due to the relatively high noise level with respect to the oscillation amplitude, which affects the SNR time series analysis. More specifically, it was observed in the GNSS simulated data that mainly for the relatively small amplitude oscillation (i.e., < 1 cm), the peak in SNR spectrum is less visible due to the noisy spectrum (Fig. 9).

The oscillation amplitude and frequency were used to construct the multipath relative phase ψ and introduced into the SNR model of (6). The latter was applied to the SNR time series by using the nonlinear least-squares method to estimate the multipath parameters (A_d, α, H_o, γ). To optimize the least-squares method, the boundaries of the multipath conditions were defined based on physical assumptions/constraints presented in Table 1. The reflector inclination was constrained to 0°–5°, assuming the ground as the reflection source based on the Fresnel zones (Zimmermann et al. 2019). The attenuation factor α was constrained between 0 and 1, covering all the cases from no reflection to strong reflection. The algorithm was iterated 50 times to estimate the parameters by checking all the potential local minima within the boundaries.

Table 1 Boundary conditions of the parameters to be estimated based on the SNR model and the SNR time series for Case A

	A_d (V)	γ (°)	H_o (m)	α
Min value	min SNR	0	1.5	0
Max value	max SNR	5	3.0	1

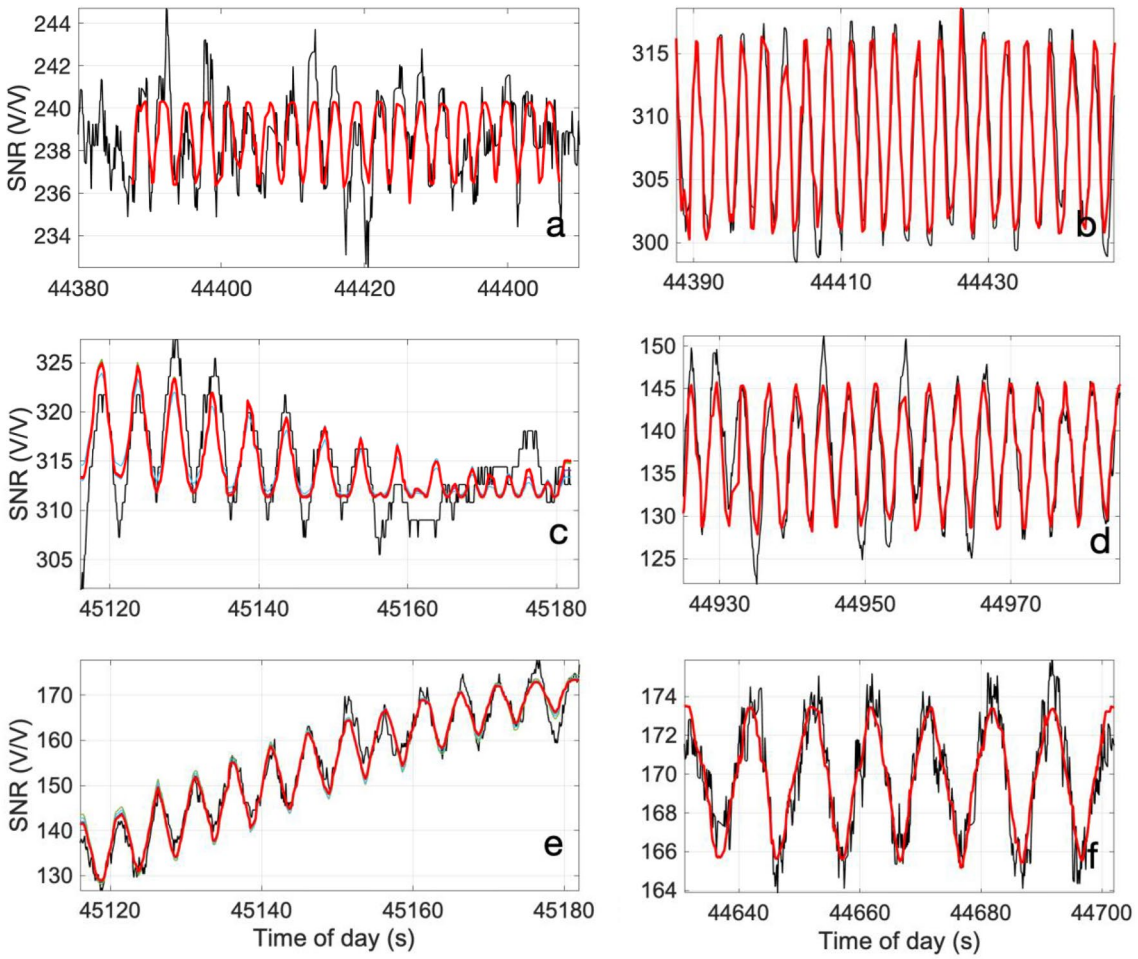

Fig. 13 SNR time series and the fit of the SNR model for **a** PRN01 and **b** PRN10 for $A_{mot} = 7.5$ mm, $f = 0.3$ Hz, **c** PRN11 for $A_{mot} = 15$ mm, $f = 0.2$ Hz, **d** PRN18 for $A_{mot} = 15$ mm, $f = 0.3$ Hz, **e** PRN22 for $A_{mot} = 15$ mm and $f = 0.2$ Hz and **f** PRN28 for $A_{mot} = 7.5$ mm and $f = 0.1$ Hz

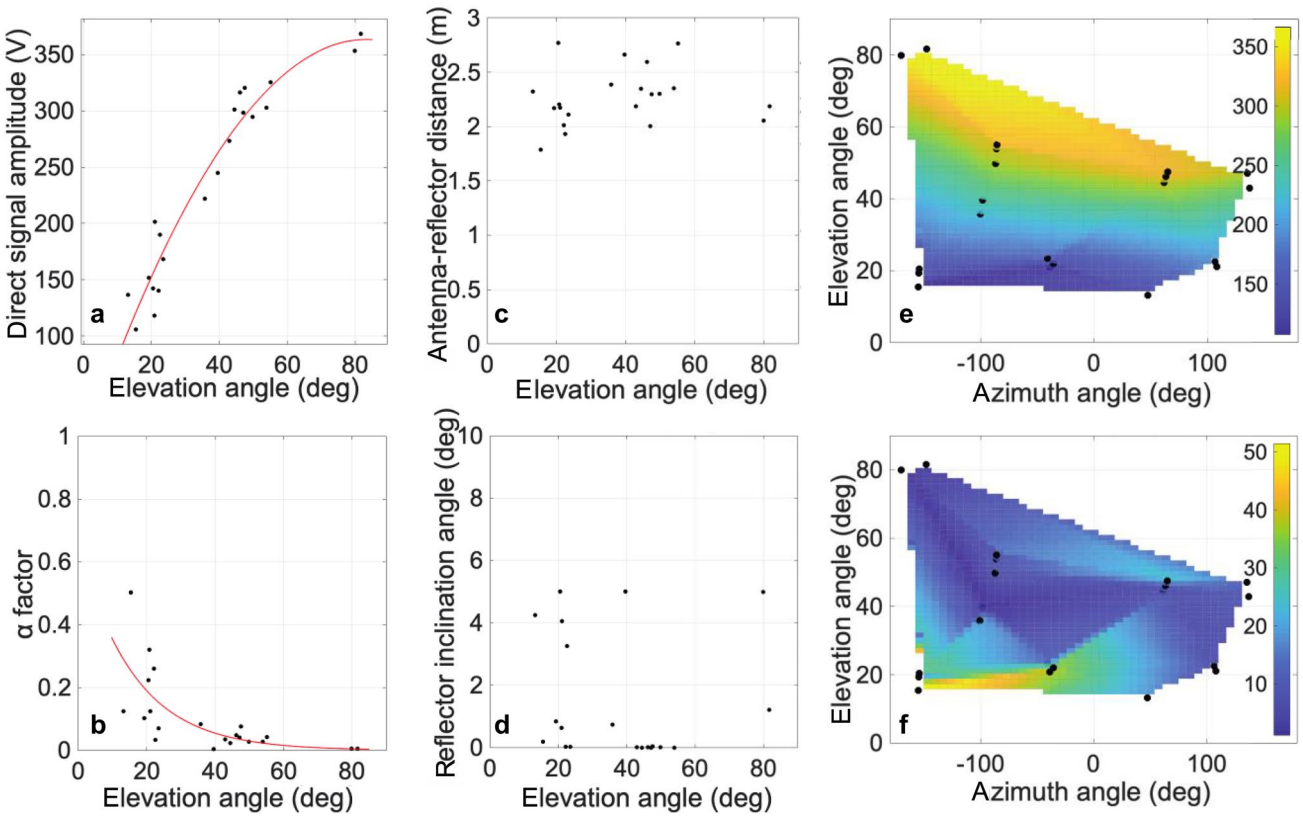

Fig. 14 Estimates of **a** the direct signal amplitude, **b** the attenuation factor α, **c** the antenna–reflector vertical distance and **d** the reflector inclination angle with respect the satellite elevation angle, as they derived from the modeling of the SNR time series for different satellites and antenna oscillation-type motions. Maps of **e** the direct and **f** the reflected signal amplitude in an azimuth versus elevation angle grid of the site. The black dots indicate the estimated values for the parameters from the modeling of the SNR time series

Figure 13 presents the SNR time series and the fitted SNR models for different satellites and oscillations. However, for oscillations of 7.5 and 15 mm, the SNR model expresses the oscillation pattern of the SNR time series successfully, even for cases where the pattern is partly generated (Fig. 13c). From the analysis of the SNR time series, the parameters (A_d, α, H_o, γ) were estimated for various satellite elevation angles. Since we assume that all satellite reflections derive from the same large horizontal surface, we combine the estimates from all satellites in Fig. 14. As it is expected, the direct satellite signal and the attenuation factor α increase and decrease, respectively, with the satellite elevation angle, as the result of the strong multipath interference from the low-elevation satellites. Both these observations are in agreement with the simulations. The estimations of the antenna–reflector distance (H_o) range between 2 and 2.5 m, whereas the majority of the estimates (~ 70%) of the reflector inclination angle is smaller than 1° (i.e., ground reflections). By pairing the estimates of the direct/reflected satellites signal with the satellite position (elevation angle and azimuth), the satellite signal-intensity maps are produced for the GNSS antenna site, where the satellite signal is strong (> 200 V) for satellite elevation angles greater than 40°. In contrast, the reflected satellite signal is strong for low-elevated satellites (< 20°) at the west side of the antenna. These maps are only indicative, due to the limited sky coverage.

Table 2 Boundary conditions for the parameters to be estimated for Case B. The parameters A_d and α are constrained by the fit of the models in Fig. 14a, b and the corresponding satellite elevation angle

	A_{mot} (mm)	γ (°)	H_o (m)		A_d (V)	α
Min value	1	0	1.5	Boundaries based on the fit of Fig. 14a, b	±40	±0.05
Max value	30	5	3.0			

Satellite data with broader coverage are needed to create a more accurate signal-intensity map.

Case B: modeling the antenna oscillation and the multipath conditions

The same methodology was followed to estimate the oscillation characteristics and the multipath conditions, where the four multipath parameters (A_d, α, H_o, γ) and the oscillation amplitude (A_{mot}) are considered unknown. The boundary conditions set for the nonlinear least square method analysis are presented in Table 2. The boundaries of parameters γ and H_o are the same with case A, whereas A_{mot} is defined between 1 and 30 mm. The boundaries of the direct multipath signal A_d and the attenuation factor α, for the given satellite elevation angle, are defined by the trend line of Figs. 14a, b and constrained in a zone of ± 40 V and ± 0.05, respectively. Figure 15 presents SNR time series, and the fitted SNR model for four different representative satellite signals. For satellites with elevation angles less than 45° (e.g., PRN 22), there is a clear oscillation pattern with substantial amplitude leads to a good fit of the SNR model. In contrast, for satellites of high elevation angle (e.g., PRN 08), the oscillation pattern is less evident with a less clear signature due to the impact of the antenna radiation pattern and the SNR noise, increasing the difficulty of applying the SNR model. This is also confirmed by the correlation coefficient (R^2) of the fit of the SNR model to the SNR time series, as it significantly reduces with the elevation angle (Fig. S10).

Furthermore, it was observed that the error of the estimated oscillation amplitude is not related to the satellite elevation angle or azimuth and it did not exceed 2.5 cm for any type of oscillation, even for the poorly described SNR time series (e.g., PRN 08 Fig. 15b). Finally, to evaluate the impact of the multiple solution problem for the antenna height estimation, the SNR model was applied to the experimental antenna oscillations for constrained and unconstrained antenna–reflector distance and oscillation amplitude (Fig. 16). It is observed that the motion amplitude error is similar in both cases, suggesting that the inaccurate antenna–reflector distance estimation does not affect the motion amplitude estimation. In contrast, for the antenna–reflector distance estimation, the unconstrained solution may lead to gross error.

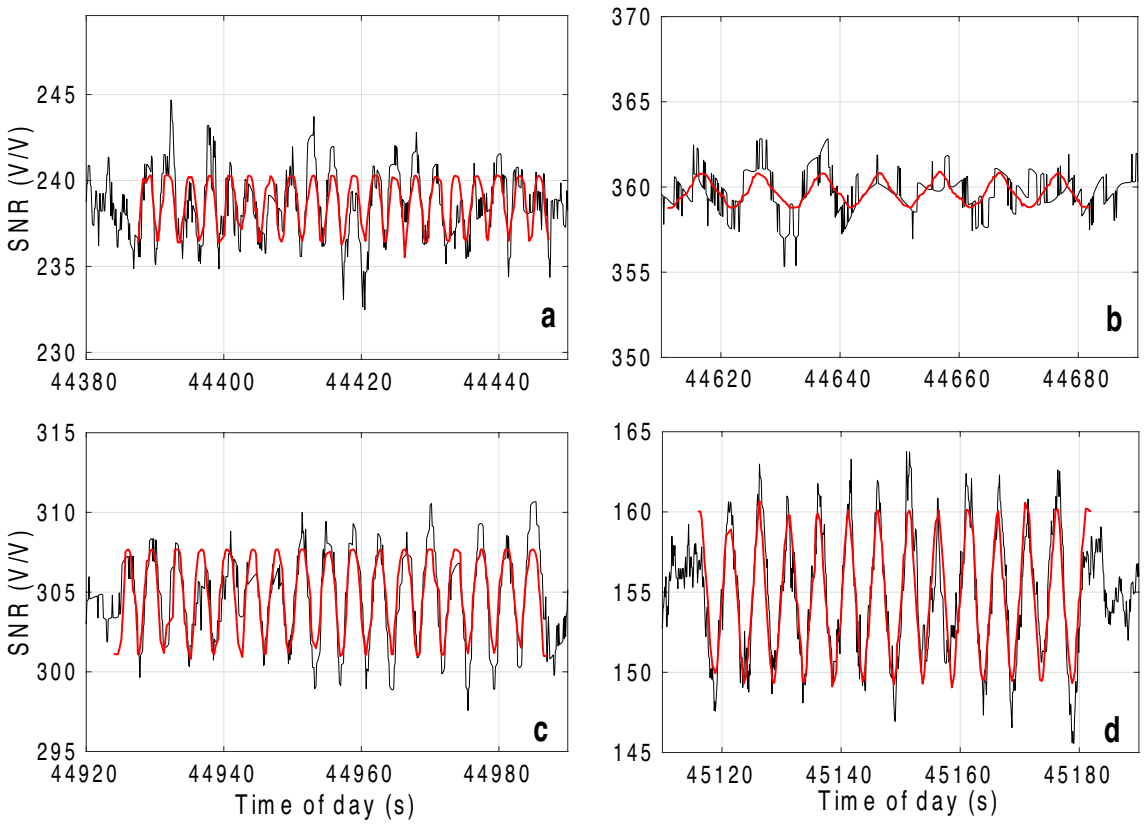

Fig. 15 SNR time series and the fit of the SNR model for **a** PRN 01 at 36° satellite elevation angle, oscillation of 7.5 mm amplitude and 0.3 Hz frequency, **b** PRN 08 at 80° satellite elevation angle, 7.5 mm amplitude and 0.1 Hz frequency, **c** PRN 10 at 45° satellite elevation angle, 15 mm amplitude and 0.3 Hz frequency and **d** PRN 22 at 19° satellite elevation angle, 15 mm amplitude and 0.2 Hz frequency

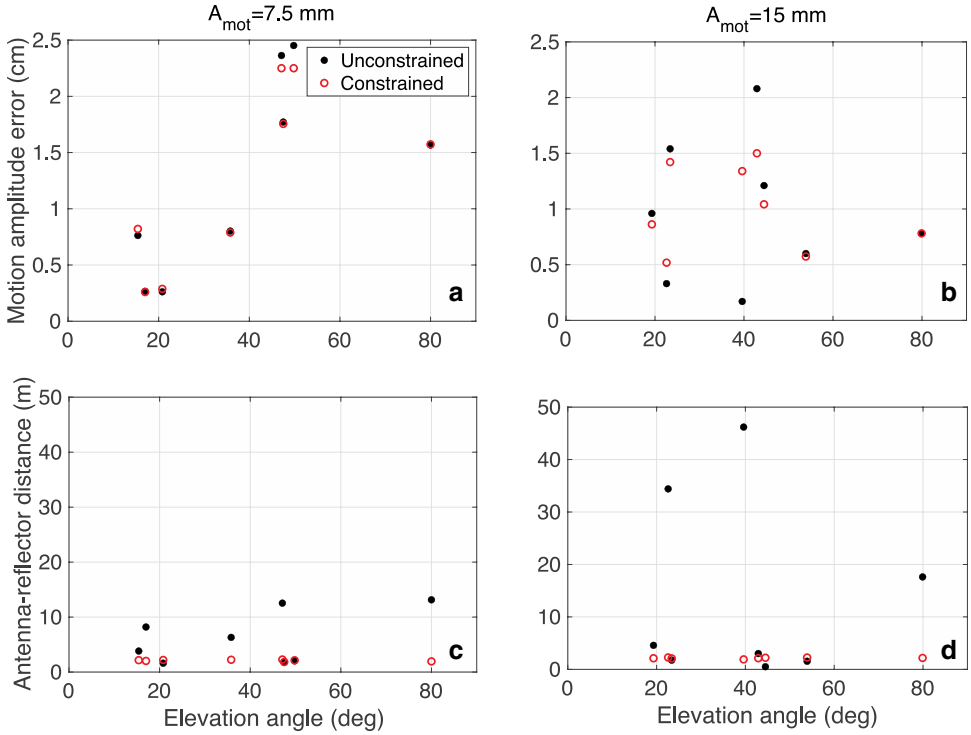

Fig. 16 **a**, **b** Antenna oscillation amplitude error and **c**, **d** estimated antenna–reflector distance with respect the satellite elevation angle for the cases of with and without boundary conditions for the antenna–reflector distance. The oscillation amplitude is 7.5 mm (**a**, **c**) and 15 mm (**b**, **d**)

Discussion

The impact of the multipath-induced SNR time series pattern for a vertical GNSS antenna oscillation was investigated through the analysis of the mathematical model, simulations and controlled experiments. All three different stages of the investigation revealed the complexity and sensitivity of the model to potential variations of the multipath intensity and geometry (A_d, α, H_o, γ, θ) and the antenna oscillation (A_{mot}, f) parameters. The main observations from the parametric analysis of the SNR model are:

- The SNR time series frequency reflects the oscillation frequency, as it was also revealed from the simulations of the experiments and highlighted by Peppa et al. (2018).
- The antenna–reflector distance affects the amplitude and the waveform of the SNR time series. The separation of the satellite motion-induced and antenna oscillation-induced multipath pattern in the SNR becomes more challenging for large antenna–reflector distance when the corresponding SNR and antenna motion frequencies tend to coincide.
- For a certain multipath intensity and ignoring the antenna radiation pattern effect, the maximum amplitude of the SNR time series depends on the elevation angle (and γ for a non-horizontal reflector), with a general increasing trend with the elevation angle and oscillation amplitude.
- The SNR time series waveform becomes more atypical but still periodic for significantly high antenna oscillation amplitude to antenna–reflector distance ratio.
- The phase shift of the SNR and the coordinate time series are zero or π.

From the analysis of the GNSS simulated data, it was proven that the variations in the SNR time series are multipath-induced, reflecting the antenna oscillation, and they were not the effect of other phenomena (Doppler effect, ionosphere, etc.; Fig. 10). The best fit of the SNR model is for relatively large oscillation amplitudes (> 2–3 cm) and low oscillation frequencies (< 1 Hz). The main problem is the SNR time series noise, which masks the low-amplitude oscillations, and the poor SNR time series resolution, which may lead to a poorly description of the multipath-induced oscillation pattern. The relatively poor SNR resolution is a barrier for effective frequency-based filtering of the SNR time series, which could potentially reduce the SNR noise and enhance the fit of the SNR model. The SNR model fits better in a strong multipath environment, as the oscillation amplitude in the SNR time series increases with the multipath strength. Furthermore, the SNR model converges to one solution for the oscillation amplitude but several solutions (differ by multiples of a specific value) for the antenna–reflector distance.

Finally, the controlled experiments confirmed the findings of the simulations. They revealed that satellites of relatively low-elevation angles could more reliably determine the

multipath conditions and/or the oscillation characteristics for a typical geodetic antenna. Still, the antenna–reflector distance is the most challenging parameter to estimate due to the multiple-converged solutions. It should be noted that the developed approach was examined for small oscillation amplitudes, not exceeding 15 mm, and the corresponding error of estimation was less than 2.5 cm.

Conclusions

The current study confirmed the hypothesis that short-time-period oscillations of the GNSS antenna are reflected in the SNR time series induced by the multipath. This new approach can broaden the multipath-related applications depending on the known conditions. In the current study, a first attempt was made to demonstrate the potential use of the developed approach to determine the characteristics of GNSS antenna oscillatory motion (i.e., frequency, amplitude) for deformation monitoring applications, mainly structural monitoring. The developed approach seemed to be effective for a known dominant reflecting surface (antenna–reflector distance, reflector angle), and more robust when constraints of the direct multipath amplitude A_d and the attenuation factor α are applied. This application can be useful when poor or even no GNSS solution is available. Furthermore, the developed approach seems to have the potential for GNSS remote sensing applications in determining the multipath conditions (i.e., attenuation factor and potentially antenna–reflector distance H_o), when known GNSS antenna oscillation (controlled GNSS antenna oscillation) is introduced and constraints on multipath conditions are applied. Finally, this approach can be used in urban locations to map the multipath environment, provide information on the multipath effect on individual satellite signals and enhance the GNSS positioning solution.

The proposed approach was evaluated for the simplified case of vertical oscillations and a horizontal reflector, and the initial hypothesis was proved. However, further investigation is needed to examine (1) the impact of inclined reflectors on the SNR time series, (2) the effectiveness of the SNR model for horizontal antenna oscillations and (3) the applicability in the satellite signal of other GNSS systems (Galileo, BeiDou, GLONASS). Also, further experiments are needed to enhance the robustness and effectiveness of this approach for GNSS reflectometry or structural monitoring applications. Finally, a further systematic experimental investigation needs to be conducted with different GNSS antenna types to evaluate the impact of the GNSS antenna on the SNR time series. The first results of experiments of similar oscillation-type motion on a choke-ring GNSS antenna and a smartphone that we conducted indicate that the reflection of the oscillation in the SNR time series is limited for the choke-ring antenna GNSS data and amplified for the smartphone GNSS records.

Supplementary Information The online version contains supplementary material available at https://doi.org/10.1007/s10291-023-01432-6.

Acknowledgements The authors would like to thank Dr Lukasz Bonenberg, helped with the simulations of GNSS data. This paper is benefited from constructive comments of three anonymous reviewers.

Data availability The simulated and experimental GPS raw data, including the SNR data, are available and can be downloaded online (https://doi.org/10.17639/nott.7142).

References

Betaille DF, Cross PA, Euler H-J (2006) Assessment and improvement of the capabilities of a window correlator to model GPS multipath phase errors. IEEE Trans Aerosp Electron Syst 42:705–717. https://doi.org/10.1109/TAES.2006.1642583

Bilich A, Larson KM (2007) Mapping the GPS multipath environment using the signal-to-noise ratio (SNR). Radio Sci 42:1–16. https://doi.org/10.1029/2007rs003652

Bilich A, Larson KM, Axelrad P (2008) Modeling GPS phase multipath with SNR: case study from the Salar de Uyuni. Boliva J Geophys Res 113:B04401. https://doi.org/10.1029/2007jb005194

Bilich A (2006) Improving the precision and accuracy of the geodetic GPS: applications to multipath and seismology, PhD Thesis, University of Colorado

Braasch MS (2017) Multipath. In: Teunissen PJ, Montenbruck O (eds) Springer handbook of global navigation satellite systems. Springer, Berlin. https://doi.org/10.1007/978-3-319-42928-1_15

Chew CC, Small EE, Larson KM, Zavorotny VU (2014) Effects of near-surface soil moisture on GPS SNR data: development of a retrieval algorithm for soil moisture. IEEE Trans Geosci Remote Sens 52:537–543. https://doi.org/10.1109/TGRS.2013.2242332

Hsu L-T, Jan S-S, Groves PD, Kubo N (2015) Multipath mitigation and NLOS detection using vector tracking in urban environments. GPS Solut 19(2):249–262. https://doi.org/10.1007/s10291-014-0384-6

Jin S, Qian X, Wu X (2017) Sea level change from BeiDou navigation satellite system-reflectometry (BDS-R): first results and evaluation. Glob Planet Change 149:20–25. https://doi.org/10.1016/j.gloolacha.2016.12.010

Larson KM, Nievinski FG (2013) GPS snow sensing: results from the earthscope plate boundary observatory. GPS Solutions 17(1):41–52

Lau L, Cross P (2007) Investigations into phase multipath mitigation techniques for high precision positioning in difficult environments. J Navig 60:457. https://doi.org/10.1017/s0373463307004341

Löfgren JS, Haas R, Scherneck H-G (2014) Sea level time series and ocean tide analysis from multipath signals at five GPS sites in different parts of the world. J Geodyn 80:66–80. https://doi.org/10.1016/j.jog.2014.02.012

Meng X, Nguyen DT, Owen JS, Xie J, Psimoulis P, Ye G (2019) Application of GeoSHM system in monitoring extreme wind events at the Forth Road Bridge. Remote Sens 11(23):2799. https://doi.org/10.3390/rs11232799

Moschas F, Psimoulis PA, Stiros SC (2013) GPS/RTS data fusion to overcome signal deficiencies in certain bridge dynamic monitoring projects. Smart Struct Syst 12:251–269. https://doi.org/10.12989/sss.2013.12.3_4.251

Msaewe HA, Psimoulis PA, Hancock CM, Roberts GW, Bonenberg L (2021) Monitoring the response of severn suspension bridge in the United Kingdom using multi-GNSS measurements. Struct Control Health Monit. https://doi.org/10.1002/stc.2830

Peppa I, Psimoulis P, Meng X (2018) Using the signal-to-noise ratio of GPS records to detect motion of structures. Struct Control Health Monit 25:e2080. https://doi.org/10.1002/stc.2080

Peppa I (2020) Analysis of GNSS station dynamic motion using the multipath effect: analytical, experimental approach and application, PhD Thesis, University of Nottingham

Psimoulis P, Stiros S (2012) A supervised learning computer-based algorithm to derive the amplitude of oscillations of structures using noisy GPS and robotic theodolites (RTS) records. Comput Struct 92–93:337–348. https://doi.org/10.1016/j.compstruc.2011

Roussel N, Frappart F, Ramillien G, Darrozes J, Baup F, Lestarquit L, Ha MC (2016) Detection of soil moisture variations using GPS and GLONASS SNR data for elevation angles ranging from 2° to 70°. IEEE J Sel Top Appl Earth Obs Remote Sens 9:4781–4794. https://doi.org/10.1109/JSTARS.2016.2537847

Steiner L, Meindl M, Geiger A (2019) Characteristics and limitation of GPS L1 observations from submerged antennas: theoretical investigation in snow, ice, and freshwater and practical observation within a freshwater layer. J Geodesy 93(2):267–280. https://doi.org/10.1007/s00190-018-1147x

Stiros S, Psimoulis P, Moschas F, Saltogianni V, Tsantopoulos E, Triantafyllidis P (2019) Multi-sensor measurement of dynamic deflections and structural health monitoring of flexible and stiff bridges. Bridge Struct 15:43–51. https://doi.org/10.3233/BRS-190152

Strode PRR, Groves PD (2016) GNSS multipath detection using three-frequency signal-to-noise measurements. GPS Solut 20:399–412. https://doi.org/10.1007/s10291-015-0449-1

Wei H, He X, Feng Y, Jin S, Shen F (2019) Snow depth estimation on slopes using GPS-interferometric reflectometry. Sensors 19(22):4994. https://doi.org/10.3390/s19224994

Wu X, Jin S, Chang L (2018) Monitoring bare soil freeze-thaw process using GPS-interferometric reflectometry: simulation and validation. Remote Sens 10(1):14. https://doi.org/10.3390/rs10010014

Zimmermann F, Schmitz B, Klingbeil L, Kuhlmann H (2019) GPS multipath analysis using Fresnel zones. Sensors 19(1):1–25

I. Peppa is a Ph.D. graduate of the Nottingham Geospatial Institute, the University of Nottingham, UK. Her Ph.D. study investigates the determination of the multipath environment and the GNSS antenna oscillatory motion by modeling the SNR observables of GNSS satellite signals.

P. A. Psimoulis is an Associate Professor at the Nottingham Geospatial Institute, University of Nottingham, UK. His research interests include the analysis and modeling of GNSS measurements and GNSS applications in deformation monitoring and geophysics.